AJNR

Quantitative MR Evaluation of Intracranial Epidermoid Tumors by Fast Fluid-attenuated Inversion Recovery Imaging and Echo-planar Diffusion-weighted Imaging

Shuda Chen, Fusao Ikawa, Kaoru Kurisu, Katsunori Arita, Junko Takaba and Yukari Kanou

AJNR Am J Neuroradiol 2001, 22 (6) 1089-1096
http://www.ajnr.org/content/22/6/1089

AJNR Am J Neuroradiol 22:1089–1096, June/July 2001

Quantitative MR Evaluation of Intracranial Epidermoid Tumors by Fast Fluid-attenuated Inversion Recovery Imaging and Echo-planar Diffusion-weighted Imaging

Shuda Chen, Fusao Ikawa, Kaoru Kurisu, Katsunori Arita, Junko Takaba, and Yukari Kanou

BACKGROUND AND PURPOSE: **Quantification of MR can provide objective, accurate criteria for evaluation of a given MR sequence. We quantitatively compared conventional MR sequences with fast fluid-attenuated inversion recovery (fast-FLAIR) and echo-planar diffusion-weighted (DW) MR imaging in the examination of intracranial epidermoid tumors.**

METHODS: **Eight patients with surgically confirmed intracranial epidermoid tumors were examined with T1-weighted MR sequences, fast T2- and proton density–weighted dual-echo sequences, fast-FLAIR sequences, and DW echo-planar sequences. We measured the MR signal intensity and apparent diffusion coefficient (ADC) of epidermoid tumors, normal brain tissue, and CSF and calculated the tumor-to-brain and tumor-to-CSF contrast ratios and contrast-to-noise ratios (CNR). Results were compared among the five MR methods.**

RESULTS: **On fast-FLAIR imaging, the mean signal intensity of epidermoid tumors was significantly higher than that of CSF but significantly lower than that of the brain; the contrast ratio and CNR of tumor-to-CSF were 4.71 and 9.17, respectively, significantly greater than the values with conventional MR imaging. On echo-planar DW imaging, epidermoid tumors showed a remarkably hyperintense signal relative to those of the brain and CSF; the mean contrast ratio and CNR of tumor-to-CSF were 13.25 and 19.34, respectively, significantly greater than those on fast-FLAIR or conventional MR imaging. The mean ADC of epidermoid tumors was 1.197×10^{-3} mm^2/s, significantly lower than that of CSF but higher than that of brain tissues.**

CONCLUSION: **Fast-FLAIR imaging is superior to conventional MR imaging in depicting intracranial epidermoid tumors. Echo-planar DW imaging provides the best lesion conspicuity among the five MR methods. The hyperintensity of epidermoid tumors on echo-planar DW imaging is not caused by the diffusion restriction but by the T2 shine-through effect.**

Intracranial epidermoid tumors are congenital neoplasms that constitute about 1% of all intracranial tumors (1–7). They tend to occur in basal subarachnoid cisterns and ventricles, especially in cerebellopontine angles (CPA), parasellar regions, and the fourth ventricles (2, 7). Compared with the satisfactory outcome of surgical treatment of these slow-growing, biologically benign lesions, their diagnosis by imaging has remained relatively problematic. This is because on conventional or contrast-enhanced CT and MR imaging, epidermoid tumors usually exhibit poor contrast from surrounding CSF and resemble other cystic masses.

Several imaging techniques have been employed to improve the detection of these tumors, such as contrast medium CT cisternography (8), constructive interference in steady state MR sequence (MR cisternography) (9), and 3D Fourier transform fast MR imaging with steady-state free precession images (10). These imaging techniques have not become popular, however, because of either technical shortcomings (8, 10) or manufacturer-imposed limitations (9).

Fast fluid-attenuated inversion recovery (fast-FLAIR) MR imaging has been reported to be more sensitive than conventional MR imaging in detecting various intracranial diseases (11–14), but only a few investigators have reported the use of FLAIR imaging in the diagnosis of intracranial epidermoid

Received September 19, 2000; accepted after revision February 9, 2001.

From the Departments of Neurosurgery (S.C., K.K., K.A., Y.K.) and Radiology (J.T.), Hiroshima University School of Medicine, Hiroshima, and the Department of Neurosurgery (F.I.), Shimane Prefectural Central Hospital, Shimane, Japan.

This work was presented in part at the 22nd Meeting of the Japanese Computed Imaging of the Central Nervous System, Saga, 1999.

Address reprint requests to Dr. Shuda Chen, Department of Neurosurgery, Hiroshima University School of Medicine, Kasumi 1-2-3, Minami-ku, Hiroshima, 734-8551, Japan.

tumors (9, 11). Diffusion-weighted (DW) imaging has been shown to be a useful method to differentiate epidermoid tumors from arachnoid cysts, by revealing the solid nature of epidermoid tumors as opposed to the fluid properties of arachnoid cysts according to their apparent diffusion coefficients (ADC) (15, 16). Previous reports of spin-echo DW imaging have been limited, however, by motion artifacts that reduced the accuracy of imaging and compromised its clinical utility. Echo-planar DW imaging now can acquire necessary MR data within a very short time, so that these troublesome artifacts can be minimized (17–19).

The purposes of this study were to investigate intracranial epidermoid tumors with fast-FLAIR and echo-planar DW imaging and to make a quantitative comparison with conventional MR sequences.

Methods

Patients

Eight consecutive patients with intracranial epidermoid tumors, three men and five women with a mean age of 58.9 years (range, 47 to 72 years), were studied from September 1996 to May 2000. Each had a single lesion that was surgically confirmed as having solid, white or yellowish-white, flaky, and soft contents, and glistening, irregular nodular surfaces. Microscopic examinations revealed that the tumors were composed of stratified squamous epithelial capsule tissue and keratinized debris. Six cases were studied preoperatively, and the other two were imaged during postoperative follow-up. The lesion sites were CPA in four cases, the fourth ventricle in three, and the suprasellar region in one.

MR Imaging and Image Processing

A 1.5-T superconducting MR system capable of echo-planar imaging (YMS Signa Horizon, General Electric) was used to perform the conventional MR, precontrast fast-FLAIR, and echo-planar DW imaging for all patients in this series. Only axial slices were selected for assessment. The conventional MR imaging included a T1-weighted spin-echo sequence (400/8/2 [TR/TE/excitations]), fast T2- and proton density–weighted dual-echo sequences (3000/14 and 98/2 [TR/first TE $_{eff}$ and second TE $_{eff}$/excitations]) with a slice thickness of 5 mm, an interslice gap of 2.5 cm, a field of view of 22 × 16 cm, and a matrix size of 256 × 192. Contrast-enhanced T1-weighted imaging was performed only in the preoperative examinations. The FLAIR imaging was performed using fast and interleaved multisection sequences (10002/2200/148/1 [TR/TI/TE_{eff}/excitation]) with a slice thickness of 5 mm, an interslice gap of 2.5 mm, a field of view of 22 × 22 cm, and a matrix size of 256 × 192. A nonselective, 180° inversion pulse was applied to the whole brain with the inversion slab being twice as thick as the imaged volume seated centrally within this inversion band. Except for T1-weighted images, all others were obtained with flow-compensation techniques designed to correct the first-order flow motion (constant velocity, v = dx/dt). The extra gradient pulses for flow compensation were applied along the direction of slice selection (z axis).

DW imaging was performed using a single-shot, spin-echo T2-weighted echo-planar sequence with a repetition time of 1600 ms, an echo time of 126 ms, a matrix size of 128 to 256 × 128, a field of view of 24 to 36 × 24 cm, and a slice thickness of 7.5 mm with no gap. The diffusion gradients were applied in all three axes (frequency, phase, and slice-selection encoding directions) with the b values set at 250, 500, 750, and 1000 s/mm^2, respectively. At each b value, the x, y, and z single-axis DW images and a baseline image (b value = 0 s/mm^2) were acquired, and the synthetic all-axes DW images were calculated automatically by the MR machine. We obtained 10 slices with 50 images at each b value within 12 to 19 seconds. Thus one examination of DW imaging was achieved with a total of 200 images.

The signal intensities of epidermoid tumors, adjacent brain tissue, and CSF were measured during conventional MR and FLAIR imaging in the regions of interest (ROIs) on the operating display of the MR machine. Circle or oval ROIs with variable size were used to cover as much of the tumor area as possible. Care was paid to minimize partial volume effect by setting the ROIs approaching but not exceeding the tumor margins. ROIs of adjacent brain tissue were set in the abutting or neighboring brain stem, cerebellum, and cerebral tissues in the same slice with the lesions. The ROIs of CSF were settled in the surrounding cisterns and fourth ventricles also in the same slices with the lesions. On FLAIR images, however, the ROIs of CSF were collected not only in the regions near the tumors but also in the distant lateral ventricles or large sylvian fissures, because of the CSF flow artifacts sometimes seen in the former. Thus if the CSF intensity was unevenly distributed in the measured slices, the mean CSF intensity in this slice was acquired through averaging the intensities of the two areas of the CSF with the highest and lowest intensities. For each case, the mean signal intensities of the epidermoid tumor, adjacent brain tissue, and CSF were obtained by averaging the signal intensities of the relevant ROIs in each slice.

For the DW images, signal intensity and ADC values were measured on a computer workstation (SUN Sparc 20) to which all DW imaging data had been transferred from the MR machine. A software program, MRvision (version 1.5.5), installed on this workstation generated ADC maps and quantified both the ADC values and the DW signal intensities of epidermoid tumors, adjacent brain tissue, and CSF. To avoid the contrast from diffusion anisotropy, we selected only the all-axes DW images to produce the ADC maps, by calculating the signal intensities of the DW images at different b values on a pixel-by-pixel basis. To acquire the largest diffusion weighting, we evaluated only the highest b value DW images for signal intensity. The mean ADC and DW signal intensity for each case were obtained through procedures similar to those used for conventional MR images, except the ADC of brain tissue. In this instance, we measured only the ADC of gray matter for statistical comparison, because it had less diffusion anisotropy and a higher ADC value than white matter, the cerebellum, or brain stem tissue.

Statistical Analysis

We quantitatively compared the tumor-to-brain contrast ratio, the tumor-to-brain contrast-to-noise ratio (CNR), the tumor-to-CSF contrast ratio, and the tumor-to-CSF CNR among the T1-, T2-, and proton density–weighted images, the fast-FLAIR images, and the echo-planar DW images. The tumor-to-brain contrast ratio and tumor-to-brain CNR were calculated as follows: tumor-to-brain contrast ratio = |SI of tumor − SI of brain|/SI of brain; tumor-to-brain CNR = |SI of tumor − SI of brain|/noise, where the *SI* represented the signal intensity and *noise* indicated the standard deviation of the image noise. Tumor-to-CSF contrast ratio and tumor-to-CSF CNR were calculated with similar methods. Additionally, in FLAIR images, the tumor-to-CSF contrast ratio and CNR were calculated separately according to the source of CSF intensity. For the tumor-to-CSF_{cist} contrast ratio and CNR, the SI of CSF was acquired in the cisterns or fourth ventricles near the lesions, whereas in the tumor-to-CSF_{ventr} contrast ratio and CNR, the SI of CSF was acquired from the distant lateral ventricles or sylvian fissures. The contrast ratios and CNRs also were calculated slice by slice and then case by case.

TABLE 1: Contrast ratios, CNRs of tumor-to-brain and tumor-to-CSF in epidermoid tumors

	Contrast Ratio Mean ± SD		CNR Mean ± SD	
MR Sequences	Tumor-to-Brain	Tumor-to-CSF	Tumor-to-Brain	Tumor-to-CSF
T1-weighted	0.52 ± 0.03	0.10 ± 0.08	14.97 ± 2.76	1.32 ± 1.21
T2-weighted	1.06 ± 0.11	0.03 ± 0.02	23.80 ± 3.78	1.56 ± 0.85
Proton density-weighted	0.10 ± 0.07	0.11 ± 0.07	3.28 ± 2.03	3.71 ± 1.81
$FLAIR_{cist}$*	0.36 ± 0.16	1.54 ± 0.74	6.05 ± 2.68	6.14 ± 2.70
$FLAIR_{ventr}$†	—	4.71 ± 1.60	—	9.17 ± 3.32
DW	1.30 ± 0.53	13.25 ± 3.67	11.51 ± 3.79	19.34 ± 5.22

* The signal intensity of CSF was measured in the surrounding arachnoid cisterns of fourth ventricles with the epidermoid tumors.
† The signal intensity of CSF was measured in the lateral ventricles and sylvian fissures.

TABLE 2: Mean ADC Values and signal intensity on FLAIR of epidermoid tumor, brain tissue, and CSF

Case No./Sex/ Age (y)	ADC Values (10^{-3} mm^2/sec)			Signal intensity on FLAIR			
	Epidermoid	Gray Matter	CSF	Epidermoid	Brain	$CSF_{ventr.}$*	$CSF_{cist.}$†
1/F/47	1.191	1.126	3.280	95.8	125.4	21.2	55.6
2/F/67	0.971	0.938	3.453	146.5	140.3	24.5	75.0
3/F/52	1.089	1.036	3.577	97.6	152.8	17.1	35.2
4/M/70	1.319	1.045	3.123	74.0	113.1	11.1	23.4
5/F/64	1.203	0.985	3.884	84.0	136.9	13.6	40.8
6/M/48	1.283	1.002	3.246	50.3	109.2	12.6	32.3
7/M/72	1.461	1.001	3.739	66.1	173.9	16.9	36.7
8/F/51	1.058	0.886	3.685	222.9	295.0	25.6	57.8
Mean	1.197	1.002	3.498	104.7	155.8	17.8	44.6
(SD)	(0.158)	(0.072)	(0.268)	(55.6)	(60.0)	(5.5)	(16.8)

* The signal intensity of CSF was measured in the lateral ventricles and sylvian fissures.
† The signal intensity of CSF was measured in the surrounding arachnoid cisterns or fourth ventricles with the epidermoid tumors.

Statistical comparisons used the Student's paired *t* test and the Pearson correlation coefficient and were performed with Statview software (version 5.0) on a Macintosh PowerPC computer. The significance of the *P* value was set at .05.

Results

All epidermoid tumors in this study showed the equivalent to slightly high signal intensity relative to CSF on T1-, T2-, and proton density–weighted images and were not enhanced after contrast infusion. On FLAIR imaging, epidermoid tumors showed signal intensities between those of brain tissue and CSF in seven cases and a minimally hyperintense signal relative to the brain in the remaining case. All epidermoid tumors appeared sharply hyperintense relative to the brain and CSF on echo-planar DW imaging.

The contrast ratios of both the tumor-to-brain and the tumor-to-CSF on DW imaging were significantly larger than those on the other MR sequences ($P \leq .0033$), with the exception of the contrast ratio of tumor-to-brain between DW images and T2-weighted images ($P = .2565$ [Table 1]). The mean contrast ratio of tumor-to-CSF on FLAIR imaging was significantly larger than that on conventional MR imaging ($P \leq .0009$). On the FLAIR sequence, the contrast ratio of tumor-to-CSF_{ventr} was significantly larger than that of tumor-to-CSF_{cist} ($P \leq .0001$).

The mean CNRs of tumor-to-brain differed significantly among the five MR methods ($P \leq .0412$ [Table 1]). As for the CNRs of tumor-to-CSF, DW images exhibited the largest mean value compared with the other MR methods ($P \leq .0035$). On FLAIR images, the mean CNR of tumor-to-CSF_{ventr} was significantly larger than that of tumor-to-CSF_{cist} ($P = .0008$). Moreover, the mean CNR of tumor-to-CSF_{ventr} on FLAIR imaging was significantly larger than that of tumor-to-CSF on proton density–weighted images ($P = .0024$), whereas there was no significant difference between the mean CNR of tumor-to-CSF_{cist} on FLAIR imaging versus proton density–weighted imaging ($P = .0622$).

The mean ADC of epidermoid tumors was significantly lower than that of CSF ($P < .0001$) and significantly higher than that of gray matter ($P = .007$ [Table 2]).

The mean CNR of tumor-to-CSF_{ventr} on FLAIR images varied from 4.97 to 14.70 and inversely correlated to the ADC values of the epidermoid tumors in the corresponding cases (Pearson correlation coefficient, −.910; $P = .0006$ [Fig 1]).

The mean signal intensity between CSF_{cist} and CSF_{ventr} differed significantly ($P = .0004$ [Table 2]). The mean signal intensity of epidermoid tumors was significantly higher than that of CSF_{cist} ($P = .0075$) and significantly lower than that of surrounding brain tissue ($P = .0032$).

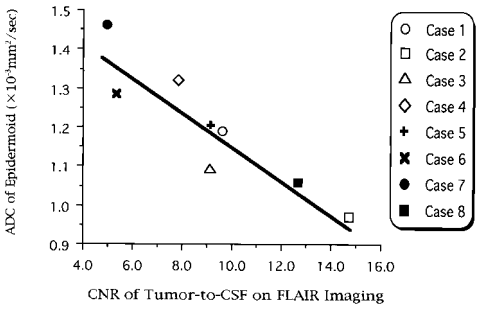

FIG 1. Inverse correlation between CNR of tumor-to-CSF_{ventr} on FLAIR images and ADC of epidermoid tumors in the corresponding cases (Pearson correlation coefficient, −.910; $P = .0006$).

Discussion

Our study shows that conventional MR imaging offers minimal tumor-to-CSF contrast ratio and CNR and is inferior to fast-FLAIR and echo-planar DW imaging in detecting intracranial epidermoid tumors.

Conventional MR Imaging

Conventional MR imaging, such as T1-, T2-, and proton density–weighted sequences, has been thought to be superior to radiographs, CT, and angiography in the diagnosis of intracranial epidermoid tumors (3, 7, 20–24), largely because of its capacity for multiplanar imaging, the lack of artifacts from bone, and clear delineation of surrounding neurovascular structures rather than its potential to demarcate the lesions. On conventional MR imaging, however, most intracranial epidermoid tumors exhibit a signal intensity that is similar to that of CSF and is not enhanced after contrast administration (Fig 2A–C). These MR characteristics made it difficult to differentiate epidermoid tumors from surrounding CSF or arachnoid cysts. It also is difficult to detect small epidermoid tumors or postoperative residual and recurrent tumors. Although the signal intensity of epidermoid tumors differs to some degree from that of CSF on conventional MR imaging, particularly on proton density–weighted images (2, 7, 23, 25, 26), this difference usually is slight and inconstant. In the diagnosis of intracranial epidermoid tumors by conventional MR imaging alone, the patient's history, the lesion's site and shape, the surrounding deformed but uninvaded brain tissue, and the lack of brain edema probably are more important than the minor differences in signal intensity between the tumor and CSF. Some investigators who have emphasized that epidermoid tumors can be discriminated from CSF on the basis of signal intensity differences on conventional MR imaging have been unable to avoid the occasional misdiagnosis (26, 27). We agree with the viewpoint that the greatest value of conventional MR imaging in the diagnosis of epidermoid tumors is its assistance in planning the surgical approach and not its capacity for ascertaining pathologic diagnosis (20, 22, 23, 28).

FLAIR Imaging

FLAIR imaging, characterized by heavy T2 weighting and CSF signal-nulling, was thought to have great potential in depicting epidermoid tumors by suppressing the signal of surrounding CSF and intensifying the long-T2 quality of the lesions. In our study, all epidermoid tumors showed significantly hyperintense signals relative to CSF, from which the lesions certainly could be discriminated, although they also had uneven intensities or showed unclear tumor margins (Fig 2D). The contrast ratio and CNR of tumor-to-CSF_{ventr} on FLAIR images also were significantly higher than that on conventional MR imaging.

A problem that requires careful treatment in FLAIR imaging of epidermoid tumors, however, is the increased signal intensity of surrounding CSF in the subarachnoid cisterns and ventricles. In our FLAIR imaging series, the mean signal intensities of CSF in these areas were higher than those in lateral ventricles or sylvian fissures. This reduced the contrast ratio and CNR of tumor-to-CSF_{cist}, and statistical analysis indicated that they could not be treated as true contrast ratios and CNRs of tumor-to-CSF. On observation, the increase in CSF signal intensity was attributable mainly to the flow artifacts of noninverted CSF, although we could not exclude partial volume effect because the CSF cisterns usually were small and narrow. Despite using the flow-compensation sequences and nonselective inversion pulse in FLAIR imaging, we could not completely exclude the CSF artifacts, especially in the infratentorial subarachnoid cisterns and ventricles, where the epidermoid tumors tended to grow. These artifacts varied in signal intensity from hypointense to hyperintense relative to brain tissue, and they occasionally simulated epidermoid tumors in shape and intensity. Thus a lesion's existence and extension might be misinterpreted (Figs 3A and 4A). In all, of 23 slices with epidermoid lesions in our FLAIR series, seven slices (30.4%) in four patients appeared to contain CSF artifacts, of which three slices (13%) contained artifacts difficult to distinguish from epidermoid tumors (Figs 3A and 4A). The use of the cardiac-gated sequence or thicker slab of 180° inversion pulse may reduce CSF artifacts on FLAIR imaging, although scanning time would be increased. Additional coronal or sagittal imaging also is likely to eliminate artifacts on the axial image.

Another noticeable point in FLAIR imaging of epidermoid tumors is that the tumors were not as hyperintense relative to the brain as on T2-weighted images, but only of intermediate intensity between the brain and CSF or minimally hyperintense relative to the brain. As a result, the contrast ratio and CNR of tumor-to-brain were lower on FLAIR images than on normal T2-weighted images. Considering the long-T1 properties of epidermoid tumors, this probably is attributable to the intrinsic T1 weighting effect in FLAIR sequences. Another

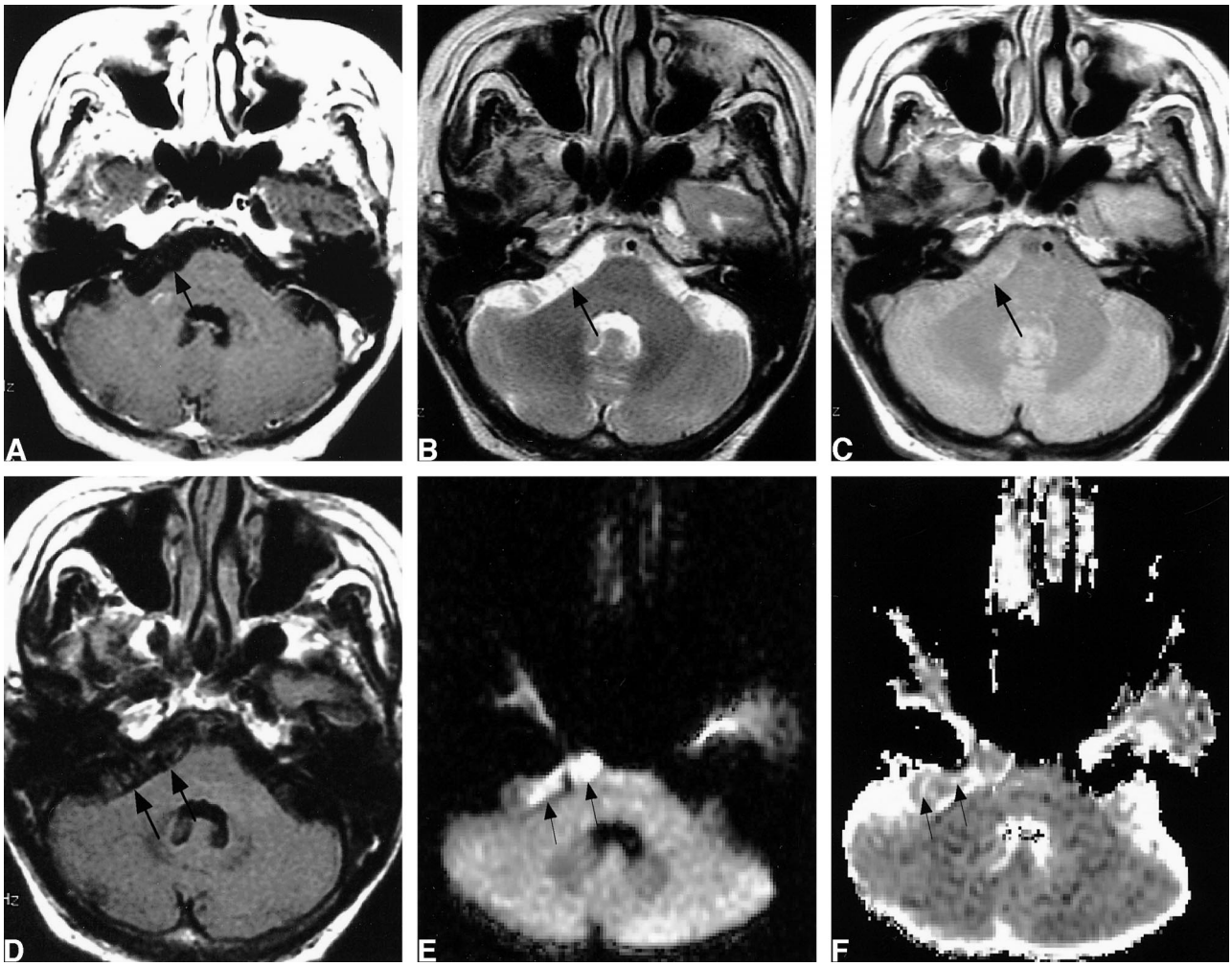

FIG 2. Right CPA epidermoid tumor in a 72-year-old man.

A-C, Contrast-enhanced T1-weighted (400/8/2 [TR/TE/excitations]) (*A*), fast T2-weighted (3000/98/2) (*B*) and proton density–weighted (3000/14/2) (*C*) images do not show the epidermoid tumor but only slight expansion of the arachnoid cistern in the right CPA (*arrow*).

D, Fast-FLAIR imaging (10002/148/1, inversion time of 2200) shows the tumor (*arrows*) as unevenly hyperintense relative to the CSF but hypointense relative to the brain.

E, Echo-planar DW imaging (1600/126 [TR/TE] with b value of 1000 s/mm^2; field of view, 24 $\times$ 24 cm) reveals the tumor as a sharply hyperintense lesion (*arrows*) relative to the brain and CSF.

F, ADC map shows that the intensity of the tumor is similar to that of surrounding brain tissue but much different from that of CSF. Note the uneven diffusion in the lesion (*arrows*).

explanation may be that epidermoid tumors usually have irregular, multilobular surfaces that sometimes insinuate deeply into the lesions and form CSF interstices (2), whose signal then could be suppressed by FLAIR sequences (Fig 2D).

We also noted that the mean CNR of tumor-to-CSF_{ventr} varied among cases and was inversely correlated with the corresponding ADC of the epidermoid tumors (Fig 1), indicating that the CNR value of tumor-to-CSF on FLAIR imaging somehow is associated with water diffusion within the lesions. Ikushima et al (9) have suggested that CNR values are inversely proportional to the hydration of the tumors. We believe that hydration depends in part on the number of CSF interstices in the lesions. The degree of hydration in the epidermoid parenchyma also should be considered.

DW Imaging

DW imaging can map contrast that reflects the molecular diffusion of water (Brownian motion) in the examined tissues. Diffusion can be quantitatively evaluated by the ADC, which is independent from proton density, T1, and T2 relaxation effects. Tsuruda and Maeda reported in succession that DW imaging could differentiate epidermoid tumors from other cystic lesions, in that the ADCs of epidermoid tumors were similar to that of brain tissue whereas the ADCs of cystic lesions were similar to that of CSF (15, 16). Both investigators, however, used a non–echo-planar DW sequence, the imaging accuracy of which can be degraded by motion artifacts. Moreover, they did not present either the DW images or the absolute ADC values. Recently, Dechambre et al (29) illustrated the echo-planar

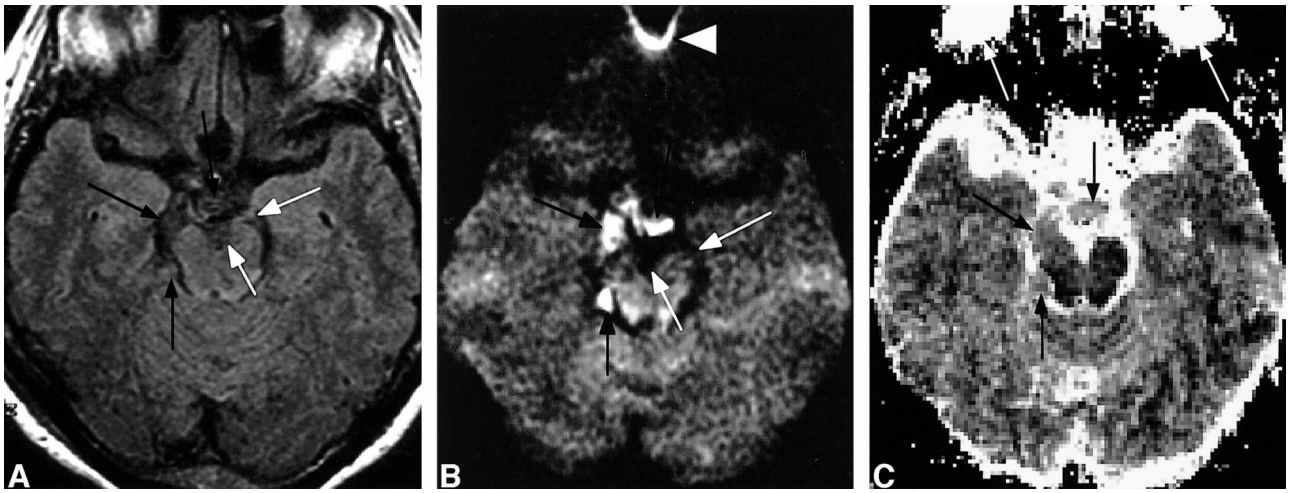

FIG 3. Suprasellar region epidermoid tumor in a 47-year-old woman.

A, Fast-FLAIR imaging (10002/148/1, inversion time of 2200) shows that epidermoid tumor (*black arrows*) fills the suprasellar and right ambient cisterns; the hyperintensity in the left ambient and interpeduncular cisterns (*white arrows*) probably is caused by CSF flow artifacts.

B, Echo-planar DW imaging (1600/126 with b value of 1000 s/mm^2; field of view, 36 $\times$ 24 cm) clearly shows that the tumor (*black arrows*) is in the suprasellar and right ambient cisterns; the signal in the left ambient and interpeduncular cisterns (*white arrow*) is greatly attenuated, indicating a fluid nature. Note the susceptibility artifacts (*white arrowhead*) at the anterior skull base.

C, ADC map shows that the ADC of the tumor (*black arrows*) is similar to that of surrounding brain tissue; the ADCs of left ambient and interpeduncular cisterns are similar to that of the eyes (*white arrows*).

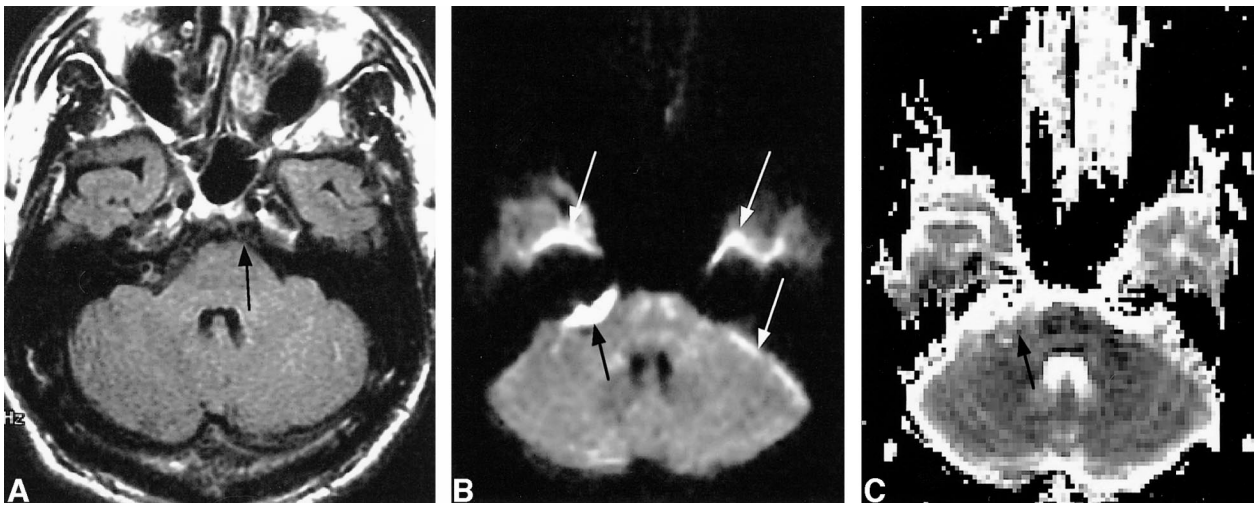

FIG 4. Right CPA epidermoid tumor in a 48-year-old man.

A, On fast-FLAIR imaging (10002/148/1, inversion time of 2200), epidermoid tumor appears to extend over the midline in the prepontine cistern (*arrow*).

B, Echo-planar DW imaging (1600/126 with b value of 1000 s/mm^2; field of view, 36 $\times$ 24 cm) reveals that the lesion (*black arrow*) is limited in the right CPA. Note the susceptibility artifacts near the temporal bone (*white arrows*).

C, ADC map shows that the tumor (*arrow*) has an ADC similar to that of surrounding brain tissue.

DW images of a single epidermoid tumor and reported its ADC value as 1090 (($\pm$200) $\times$ (10^{-6} mm^2/s.

On echo-planar DW imaging in our study, all epidermoid tumors appeared sharply hyperintense relative to the brain and CSF. The contrast ratio and CNR of tumor-to-CSF were as much as several to 100 times the values on FLAIR and conventional MR images. In our practical observation, echo-planar DW imaging had the best tumor conspicuity among the five MR methods; in particular, it greatly aided in evaluation of the postoperative patients. On conventional MR imaging, postoperative changes in the surgical cavity usually make the detection of residual tumor or recurrence more difficult (30, 31). Our study revealed that the mean ADC of epidermoid tumors was 1.197 $\times$ 10^{-3} mm^2/s, higher than that of gray matter, implying more active diffusion in the epidermoid tumors than in the brain parenchyma. On ADC mapping with a small field of view, eg, 24 $\times$ 24 cm, epidermoid tumors showed uneven signal intensity patterns, suggesting uneven proton diffusion (Fig 2F). Considering that CSF interstices may invaginate into the lesions, the ADC

of epidermoid parenchyma might be closer to that of brain tissue. Nonetheless, the ADC values of epidermoid tumors were much different from that of CSF, which helps avoid confusing the tumors with CSF or arachnoid cysts.

DW imaging is designed to depict the mobility of water molecules in the imaged section; however, the signal intensity on DW images does not simply represent the water diffusibility (ADC). Because DW imaging basically is a diffusing proton-attenuated T2-weighted sequence with a given b value, DW contrast depends not only on the ADC but also on the T2 values and even, although only slightly, on the proton density of the examined tissues (32). A tissue's DW signal intensity inversely correlates with its diffusibility or ADC but directly correlates with its T2 values and proton density. In our study, epidermoid tumors showed a mean DW signal intensity 130% higher than that of brain tissue; however, without exception, the ADCs of epidermoid tumors were not lower but higher than that of the brain. Apparently, this hyperintensity on DW imaging should not be attributed to a decrease in ADC. Because of the remarkable T2 prolongation, the DW hyperintensity of epidermoid tumors should be attributed to the T2 shine-through effect (32, 33), meaning that the T2 properties dominated the contributions to the DW signal intensity and even overwhelmed the effect of signal attenuation resulting from the increase in ADC. The T2 shine-through effect also is found in subacute cerebral infarction (32, 33) and other brain tumors; however, to our knowledge, there have not been examples of intracranial tumors with T2 shine-through phenomenon showing such intense contrast between the lesion and brain as the epidermoid tumors.

Echo-planar DW imaging did have its disadvantages. Because of the strong diffusion gradients, the signal-to-noise ratio and tissue contrast were much reduced, resulting in poor anatomic delineation of the cerebral structures. This made conventional MR imaging indispensable in planning surgical procedures. Other limitations were the artifact and anatomic distortion caused by susceptibility effects in the echo-planar sequence. They usually happened in regions rich in air-bone interfaces, such as the anterior and mid-skull bases, and were identified easily (Figs 3B and 4B).

Limitations

A limitation of our study is that we included only cases in which the lesions exhibited a classic appearance on conventional MR imaging. Several reports have described unusual MR imaging findings of intracranial epidermoid tumors, in which the lesions have shown, relative to the brain, a hyperintense signal on T1-weighted images, a hypointense signal on T2-weighted images, a mixed signal intensity on T1- and T2-weighted images, and no signal on T2-weighted and proton density–weighted images (28, 34–38). As reported, these variations in MR signal intensity resulted from the different chemical components and physical states of the lesion contents. It is reasonable to believe that differences in contents will cause variations not only in the T1, T2, and proton density properties but also in the ADC values of epidermoid tumors. We speculate that these unusual epidermoid tumors likewise may show diverse MR signal intensities and ADC values on fast-FLAIR and echo-planar DW images, according to the different chemical components and physical states of lesion contents.

Conclusion

Fast-FLAIR imaging is superior to conventional MR imaging in depicting intracranial epidermoid tumors, showing variable but satisfactory lesion contrast to both CSF and brain tissue. It may give an incorrect demarcation of the lesion, however, because of CSF flow artifacts. Echo-planar DW imaging reveals intracranial epidermoid tumors as hyperintense lesions relative to the brain and CSF and has the best conspicuity of the five MR methods tested. The hyperintensity of epidermoid tumors on echo-planar DW imaging is not caused by diffusion restriction in the lesions but by the intrinsic T2 shine-through effect on the diffusion-weighted MR sequence.

References

1. Conley FK. **Epidermoid and dermoid tumors: clinical features and surgical management.** In: Wilkins RH, Rengachary SS, eds. *Neurosurgery* 2nd ed. New York, NY: McGraw-Hill, Health Professions Division; 1996;971–976
2. Gao PY, Osborn AG, Smirniotopoulos JG, Harris CP. **Radiologic-pathologic correlation. Epidermoid tumor of the cerebellopontine angle.** *AJNR Am J Neuroradiol* 1992;3:863–872
3. Vion-Dury J, Vincentelli F, Jiddane M, et al. **MR imaging of epidermoid cysts.** *Neuroradiology* 1987;29:333–338
4. Yasargil MG, Abernathey CD, Sarioglu AC. **Microneurosurgical treatment of intracranial dermoid and epidermoid tumors.** *Neurosurgery* 1989;24:561–567
5. Yamakawa K, Shitara N, Genka S, Manaka S, Takakura K. **Clinical course and surgical prognosis of 33 cases of intracranial epidermoid tumors.** *Neurosurgery* 1989;24:568–573
6. Altschuler EM, Jungreis CA, Sekhar LN, Jannetta PJ, Sheptak PE. **Operative treatment of intracranial epidermoid cysts and cholesterol granulomas: report of 21 cases.** *Neurosurgery* 1990;26: 606–614
7. Mohanty A, Venkatrama SK, Rao BR, Chandramouli BA, Jayakumar PN, Das BS. **Experience with cerebellopontine angle epidermoids.** *Neurosurgery* 1997;40:24–29
8. Fein JM, Lipow K, Taati F, Lansem T. **Epidermoid tumor of the cerebellopontine angle: diagnostic value of computed tomographic metrizamide cisternography.** *Neurosurgery* 1981;9: 179–182
9. Ikushima I, Korogi Y, Hirai T, et al. **MR of epidermoids with a variety of pulse sequences.** *AJNR Am J Neuroradiol* 1997;18: 1359–1363
10. Sakamoto Y, Takahashi M, Ushio Y, Korogi Y. **Visibility of epidermoid tumors on steady-state free precession images.** *AJNR Am J Neuroradiol* 1994;15:1737–1744
11. Tsuchiya K, Mizutani Y, Hachiya J. **Preliminary evaluation of fluid-attenuated inversion-recovery MR in the diagnosis of intracranial tumors.** *AJNR Am J Neuroradiol* 1996;17:1081–1086
12. Rydberg JN, Hammond CA, Grimm RC, et al. **Initial clinical experience in MR imaging of the brain with a fast fluid-attenuated inversion-recovery pulse sequence.** *Radiology* 1994;193: 173–180

13. Essig M, Knopp MV, Schoenberg SO, et al. **Cerebral gliomas and metastases: assessment with contrast-enhanced fast fluid-attenuated inversion-recovery MR imaging.** *Radiology* 1999; 210:551–557
14. Bastianello S, Bozzao A, Paolillo A, et al. **Fast spin-echo and fast fluid-attenuated inversion-recovery versus conventional spin-echo sequences for MR quantification of multiple sclerosis lesions.** *AJNR Am J Neuroradiol* 1997;18:699–704
15. Tsuruda JS, Chew WM, Moseley ME, Norman D. **Diffusion-weighted MR imaging of the brain: value of differentiating between extraaxial cysts and epidermoid tumors.** *AJNR Am J Neuroradiol* 1990;11:925–931
16. Maeda M, Kawamura Y, Tamagawa Y, et al. **Intravoxel incoherent motion (IVIM) MRI in intracranial, extraaxial tumors and cysts.** *J Comput Assist Tomogr* 1992;16:514–518
17. Tien RD, Felsberg GJ, Friedman H, Brown M, MacFall J. **MR imaging of high-grade cerebral gliomas: value of diffusion-weighted echoplanar pulse sequences.** *AJR Am J Roentgenol* 1994;162:671–677
18. Ebisu T, Tanaka C, Umeda M, et al. **Hemorrhagic and nonhemorrhagic stroke: diagnosis with diffusion-weighted and T2-weighted echo-planar MR imaging.** *Radiology* 1997;203: 823–828
19. Noguchi K, Nagayoshi T, Watanabe N, et al. **Diffusion-weighted echo-planar MRI of lacunar infarcts.** *Neuroradiology* 1998;40: 448–451
20. Olson JJ, Beck DW, Crawford SC, Menezes AH. **Comparative evaluation of intracranial epidermoid tumors with computed tomography and magnetic resonance imaging.** *Neurosurgery* 1987;21:357–360
21. Steffey DJ, De Filipp GJ, Spera T, Gabrielsen TO. **MR imaging of primary epidermoid tumors.** *J Comput Assist Tomogr* 1988; 12:438–440
22. Rubin G, Scienza R, Pasqualin A, Rosta L, Da Pian R. **Craniocerebral epidermoids and dermoids. A review of 44 cases.** *Acta-Neurochir (Wien)* 1989;97:1–16
23. Tampieri D, Melanson D, Ethier R. **MR imaging of epidermoid cysts.** *AJNR Am J Neuroradiol* 1989;10:351–356
24. Gormley WB, Tomecek FJ, Qureshi N, Malik GM. **Craniocerebral epidermoid and dermoid tumours: a review of 32 cases.** *Acta-Neurochir (Wien)* 1994;128:115–121
25. Kallmes DF, Provenzale JM, Cloft HJ, McClendon RE. **Typical and atypical MR imaging features of intracranial epidermoid tumors.** *AJR Am J Roentgenol* 1997;169:883–887
26. Vinchon M, Pertuzon B, Lejeune JP, Assaker R, Pruvo JP, Christiaens JL. **Intradural epidermoid cysts of the cerebellopontine angle: diagnosis and surgery.** *Neurosurgery* 1995;36:52–57
27. Gandon Y, Hamon D, Carsin M, et al. **Radiological features of intradural epidermoid cysts. Contribution of MRI to the diagnosis.** *J Neuroradiol* 1988;15:335–351
28. Ishikawa M, Kikuchi H, Asato R. **Magnetic resonance imaging of the intracranial epidermoid.** *Acta Neurochir (Wien)* 1989; 101:108–111
29. Dechambre S, Duprez T, Lecouvet F, Raftopoulos C, Gosnard G. **Diffusion-weighted MRI postoperative assessment of an epidermoid tumor in the cerebellopontine angle.** *Neuroradiology* 1999;41:829–831
30. Lunardi P, Fortuna A, Cantore G, Missori P. **Long-term evaluation of asymptomatic patients operated on for intracranial epidermoid cyst-comparison of the diagnostic value of magnetic resonance imaging and computer-assisted cisternography for detection of cholesterin fragments.** *Acta Neurochir (Wien)* 1994; 128:122–125
31. Talacchi A, Sala F, Alessandrini F, Turazzi S, Bricolo A. **Assessment and surgical management of posterior fossa epidermoid tumors: report of 28 cases.** *Neurosurgery* 1998;42:242–252
32. Burdette JH, Elster AD, Ricci PE. **Acute cerebral infarction: quantification of spin-density and T2 shine-through phenomena on diffusion-weighted MR images.** *Radiology* 1999;212: 333–339
33. Provenzale JM, Engelter ST, Petrella JR, Smith JS, MacFall JR. **Use of MR exponential diffusion-weighted images to eradicate T2 "shine-through" effect.** *AJR Am J Roentgenol* 1999;172: 537–539
34. Kasai H, Kawakami K, Yamanouchi Y, Inagaki T, Kawamura Y, Matsumura H. **A case of pineal epidermoid cyst showing an interesting magnetic resonance imaging.** *No-Shinkei-Geka* 1990; 18:767–771
35. Horowitz BL, Chari MV, James R, Bryan RN. **MR of intracranial epidermoid tumors: correlation of in vivo imaging with in vitro ^{13}C spectroscopy.** *AJNR Am J Neuroradiol* 1990;11: 299–302
36. Gualdi GF, Biasi CD, Trasimeni G, Pingi A. **Unusual MR and CT appearance of an epidermoid tumor.** *AJNR Am J Neuroradiol* 1991;12:771–772
37. Timmer FA, Sluzewski M, Treskes M, van Rooij WJ, Teepen JL, Wijnalda D. **Chemical analysis of an epidermoid cyst with unusual CT and MR characteristics.** *AJNR Am J Neuroradiol* 1998;19:1111–1112
38. Ochi M, Hayashi K, Hayashi T, et al. **Unusual CT and MR appearance of an epidermoid tumor of the cerebellopontine angle.** *AJNR Am J Neuroradiol* 1998;19:1113–1115